Biophysical Journal Volume 96 June 2009 4755–4763

Mechanisms and Constraints on Yeast MAPK Signaling Specificity

Bo Hu, Wouter-Jan Rappel, and Herbert Levine*
Center for Theoretical Biological Physics and Department of Physics, University of California at San Diego, La Jolla, California

ABSTRACT The survival of cells relies on their ability to respond specifically to diverse environmental signals. Surprisingly, intracellular signaling pathways often share the same or homologous protein components, yet undesirable crosstalk is, in general, suppressed. This signaling specificity has been well studied in the yeast model system *Saccharomyces cerevisiae*, where the mitogen-activated protein kinase (MAPK) cascades are repeatedly employed in mediating distinct biological processes including pheromone-induced mating and filamentous growth under starvation. Although various mechanisms have been proposed to interpret the yeast MAPK signaling specificity, a consistent theory is still lacking. Here, we present a mathematical model that shows signaling specificity can arise through asymmetric hierarchical inhibition. The parameters of our model are, where possible, based on experimental data that allow us to determine the constraints imposed by signaling specificity on these parameters. Our model is in broad agreement with experimental observations to date and generates testable predictions that may stimulate further research.

INTRODUCTION

One of the central questions for biological information processing is how cells sense and distinguish extracellular stimuli when intracellular signaling components are shared among pathways. This sharing of components could potentially lead to erroneous cross-activation where the wrong downstream pathway is activated after an external stimulus. To maintain signaling specificity, cells have evolved a variety of different mechanisms (1). An obvious mechanism that leads to specificity is to physically separate the pathways. This can be done by either sequestration, where key components of the pathways bind to scaffolding proteins, or compartmentalization, where the shared component is restricted to a small portion of the cell.

In some cases, however, signaling specificity is achieved in different ways. An example can be found in the budding yeast *Saccharomyces cerevisiae*, where common protein kinases are activated during the mating pheromone signaling, the switch to filamentous growth, and the response to osmotic stress (1). Fig. 1 *A* shows the interaction between the mating and filamentous growth pathways, both of which are well characterized through extensive experimental investigations (2–4). To illustrate the potential for cross talk between these two pathways we have colored shared components in yellow. The mating pathway is activated by the α-pheromone receptor that leads to the dissociation of G protein into Gα and G$\beta\gamma$ subunits. The latter recruits the scaffold protein Ste5 to the plasma membrane, where the mitogen-activated protein kinase (MAPK) MAPKKK Ste11, the MAPKK Ste7, and the MAPK Fus3 are sequentially activated with the aid of upstream kinases including Ste20 and Ste50. MAPK Fus3 is Ste5-dependent and plays a central role in mating because it controls not only pheromone-dependent gene expression, but also promotes cell cycle arrest and mating projection (5). Among many downstream targets, Fus3 activates the transcription factor Ste12 in the nucleus by phosphorylating two redundant Ste12 inhibitors, Dig1 and Dig2 (6). Activated Ste12 proteins appear to act as dimers and drive the pheromone response elements of inducible mating genes (7,8).

The filamentous growth pathway in yeast cells is responsible for the switch to an invasive growth form under nitrogen starvation and shares many components with the mating pathway (9–11). In particular, it also possesses a MAPK cascade with identical MAPKKK and MAPKK components but with a different MAPK (Kss1). A major difference, however, is that the scaffold protein Ste5 is not needed for the activation of the filamentation-specific MAPK Kss1. Kss1 activates Ste12 as well as the filamentation-specific transcription factor Tec1; active Ste12 and Tec1 bind cooperatively to drive the filamentation response elements (12). Remarkably, Tec1 is degraded rapidly in the presence of active Fus3 after pheromone exposure, providing a unilateral inhibition to avoid cross-activation (13–15). When such negative effect of Fus3 is eliminated by mutants expressing stable Tec1, Fus3 appears to be as potent as Kss1 to activate the filamentation program upon pheromone stimulation, indicating that Fus3 has dual regulatory functions in filamentous growth (14). Finally, both pathways induce the gene *STE12*, and hence Ste12 is upregulated by itself; also, there is a positive feedback loop that upregulates Tec1, as *TEC1* is among filamentation-specific genes (16).

A variety of mechanisms at the MAPK cascade level have been proposed to interpret the specificity in yeast signaling. For example, the scaffold protein Ste5 has long been thought to promote signaling specificity by sequestration (17,18). Even though some experiments suggest that specificity is promoted by the selective activation of Ste5 (19), there are several arguments why specificity cannot arise at the

Submitted July 3, 2008, and accepted for publication February 11, 2009.

*Correspondence: hlevine@ucsd.edu

Editor: Jason M. Haugh.

0006-3495/09/06/4755/9 $2.00

doi: 10.1016/j.bpj.2009.02.065

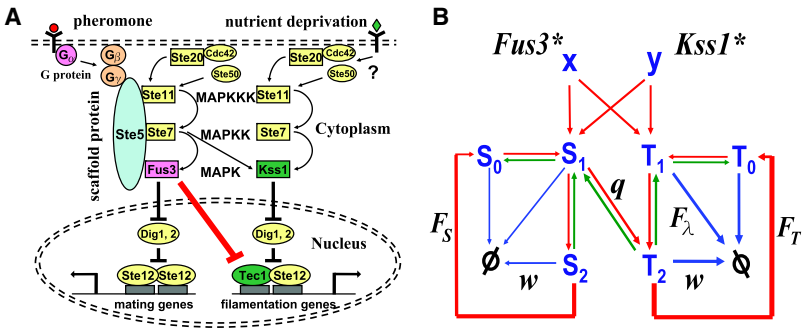

FIGURE 1 (*A*) Illustration of the mating pathway, initiated by pheromone stimulations, and the filamentous growth pathway, activated by nutrient starvation. Shared components are colored in yellow and details of the interactions can be found in the text. (*B*) Schematic representation of the core of our model with forward processes indicated in red, backward processes in green, and degradation processes in blue. As input, the model takes the Fus3* and Kss1* levels. These input variables, called x and y here, activate Ste12 and Tec1, leading to the dimers Ste12-Ste12 (S_2) and Ste12-Tec1 (T_2), the output of our model. The specificity-determining parameters are indicated and include q, controlling the relative heterodimerization rate of T_1 and S_1; w, the relative degradation rate of the dimers; F_λ, tuning the Fus3*-dependent degradation rate of Tec1; F_S, adjusting the positive feedback of the gene expression on Ste12; and F_T, determining the genetic positive feedback of Tec1.

MAPK cascade level alone, but needs to involve mechanisms operating at the gene transcription level. First of all, after pheromone stimulation the MAPKK Ste7 not only phosphorylates Fus3 but also Kss1. Activated Kss1 will phosphorylate Tec1, resulting in filamentation gene expression. How can the downstream gene regulatory circuit filter out the information transmitted by Kss1 after pheromone treatment? Secondly, although only Kss1 is phosphorylated under nutrient deprivation, Kss1 activates both Ste12 and Tec1. The activation of Ste12 is likely to drive undesirable mating-specific genes through its positive feedback loop. Again, how is the downstream specificity achieved when Ste12 could leak to the mating program?

The first question can be answered by the inhibitory function of Fus3 on Tec1. Experiments have demonstrated that activated Fus3 can suppress the activation of Tec1 by degrading it, thus providing a mechanism that prevents the onset of the filamentation pathway as a result of the activation of Kss1 through the mating signaling (13–15). The solution to the second question is less clear and needs to be sought at the downstream level. In this view, the MAPK module acts like an intermediate circuit that integrates and preprocesses environmental cues, and controls the duration and strength of the intermediate products, Fus3 and Kss1. These products can be regarded as the input for the downstream gene regulatory network.

In this article, we propose a mathematical model to study how the downstream gene regulatory network can achieve signaling specificity. Our model shows how this signaling property can be achieved through asymmetric hierarchical inhibition where the activation of the mating program is determined upstream from that of the filamentation pathway. An essential ingredient of our model is the degradation of the transcription factor dimers (Fig. 1 *B*), without which signaling specificity may be destroyed. In contrast to the mutual inhibition mechanism, hierarchical inhibition may give rise to monostable and history-independent output, as demonstrated in our simulations. The rate constants used in our model are mostly derived from experimental data and a careful examination of the parameter space reveals interesting constraints on some key parameters. In general, our simulation results are consistent with known experiments and the model generates several testable experimental predictions.

MODEL

Our model is restricted to the signaling process and gene regulation in the nucleus, with active MAP kinases Fus3* and Kss1* as the input, where * stands for activated components. The key players in our model are thus the transcription factors Ste12 and Tec1. To simplify our model, we will only consider the inactive monomers (Ste12 and Tec1, possibly bound to Dig1 and Dig2), the active monomers (Ste12* and Tec1*), and the active dimers (Ste12*-Ste12* and Tec1*-Ste12*). Note that this approach does not distinguish between inactive monomers and complexes of Ste12 and Tec1 with the abundantly present Dig1 and Dig2. In particular, it does not take explicitly into account the inactive complex Tec1-Ste12-Dig1 that can contribute to both the Tec1 concentration and the Ste12 concentration. We have verified that the inclusion of these microscopic states does not alter our results; a more detailed discussion is presented in the Model Variant section of our Supporting Material. Since the transcription factor dimers positively regulate the gene expression levels for the mating or filamentation program (1), we will take the active dimers as output variables.

In our model development, we started with a detailed representation of the two pathways (Fig. 1 *A*). This network resulted in eight equations for eight variables which take the activated Fus3*, denoted here by x, and activated Kss1* (y) as input. A full description of this model can be found in the Supporting Material. To clarify the basic mechanisms underlying signal specificity, we have reduced this full model to a more amenable four-variable model. The procedure employed in this reduction is detailed in the Supporting Material and involves quasi-steady-state approximations. Importantly, the qualitative features of the reduced and detailed model are identical. The reduced model has only four variables: the complexes containing inactive Ste12 (S_0); the active monomer Ste12* (S_1); the complexes containing inactive Tec1 (T_0); and the active monomer Tec1* (T_1). The output of this model, the Ste12*-Ste12* dimer (S_2) and the Ste12*-Tec1* dimer (T_2), can be related to the variables of the model through $S_2 = S_1^2/K_S$ and $T_2 = S_1T_1/K_T(x)$, where K_S and $K_T(x)$ are equilibrium disassociation constants for which the specific expressions can be found in the Supporting Material.

Fig. 1 *B* shows a schematic representation of the reduced model. The input x and y facilitate the activation of both S_1 and T_1, which together can form heterodimers T_2. Besides, S_1 itself dimerizes to the homodimer S_2. All forms of Ste12 and Tec1, including the dimers, can degrade. Through gene expression, there is a positive feedback from S_2 to S_0 and from T_2 to T_0. The figure also highlights the three processes that break the symmetry between the two pathways. These are:

1. The branching from Ste12 to Tec1 via the heterodimerization process $S_1 + T_1 \leftrightharpoons T_2$. This process is controlled in our model by the parameter q, which is the ratio of the on-rates for the heterodimer and homodimer. This competitive interaction is based on experimental results, which show that abolishing the interaction of Tec1 with Ste12 eliminates Tec1-mediated gene expression, suggesting that the association of Tec1 with Ste12 is responsible for the filamentation transcription activity (20). The relevant rates for these interactions are not known.
2. The Tec1 degradation, which is accelerated in the presence of Fus3* and described as a sigmoidal Fus3*-dependent function with a maximum value of F_λ. This process is based on recent experiments showing that Fus3* phosphorylates Tec1, resulting in its degradation by the SCF^{Cdc4} ubiquitin ligase (14). Different sources indicate that Tec1 has a half-life of ~15 min in the absence of pheromone treatment, and has a lifetime that is significantly smaller than 5 min after treatment with high levels of pheromone (14,15,21). Thus, a conservative estimate is that the half-life of Tec1 is shortened at least threefold in the mating program, i.e., $F_\lambda > 3$. The half-lives of Ste12, on the other hand, are much longer: at ~4 h without, and ~30 min with, pheromone treatment (22). Therefore, we treat the degradation rate of Ste12 as a constant in our model. We have verified that the inclusion of a pheromone-dependent degradation rate does not change our qualitative results (data not shown).
3. The stronger promoter activity of the *TEC1* gene relative to the promoter activity of *STE12*. Like the Tec1 degradation, the promoter activities are mathematically described as the sigmoidal Hill functions each with a maximum of F_T and F_S, respectively (see Supporting Material). The experimental picture suggests that F_S is smaller than F_T (23,24), and we have used the parameter range shown in Table S2 of the Supporting Material.

In addition to these parameters, we have also investigated the dependence of our model on a parameter w that controls the degradation of the dimers. This parameter can take on values between 0 and 1, with 0 corresponding to completely stable dimers and with 1 corresponding to a dimer decay rate equal to that of their monomers. Experimentally, Tec1 appears to interact with Ste12 via its C-terminal, whereas Fus3 binds directly to the N-terminal residues of Tec1 (13). Thus, the heterodimer Tec1*-Ste12* may be easily accessible to Fus3* and experience Fus3-mediated degradation which, as incorporated in our model, selectively degrades its Tec1* component. Little is known about the stability of the dimers, but we will see in Results that this parameter can have significant consequences.

The equations describing our reduced model can be written as

$$\frac{dS_0}{dt} = -g_S(x,y)S_0 + d_S S_1 - \lambda_S S_0 + \lambda_S S_b P_S(S_2), \quad (1)$$

$$\frac{dS_1}{dt} = g_S(x,y)S_0 - d_S S_1 - \lambda_S S_1 - 2w\lambda_S S_2 - w\lambda_T(0)T_2, \quad (2)$$

$$\frac{dT_0}{dt} = -g_T(x,y)T_0 + d_T T_1 - \lambda_T(x)T_0 + \lambda_T(0)T_b P_T(T_2), \quad (3)$$

$$\frac{dT_1}{dt} = g_T(x,y)T_0 - d_T T_1 - \lambda_T(x)T_1 - w\lambda_T(x)T_2. \quad (4)$$

Here, $g_S(x, y)$ and $g_T(x, y)$ are the input-dependent activation rates with maxima g_{Sm} and g_{Tm}, respectively; d_S and d_T are the deactivation rates; λ_S and $\lambda_T(x)$ are the degradation rates with the latter having a maximum of $F_\lambda\lambda_T(0)$; S_b and T_b are the initial concentrations of Ste12 and Tec1; and $P_S(S_2)$ and $P_T(T_2)$ are the promoter activities for *STE12* and *TEC1* with maxima F_S and F_T, respectively. Explicit expressions for the rates can be found in the Supporting Material where the parameter values are listed in Table S2. Note that the degradation rate in the last term in Eq. 2 is independent of x, in contrast to the last term in Eq. 4. This result, which follows from the quasi-steady-state approximation, reflects the different degradation rates of Ste12 and Tec1 after pheromone stimulation. For more details of the model assumptions and the quasi-steady-state approximation, we refer to the Supporting Material.

These equations were integrated using MatLab 7 (The MathWorks, Natick, MA). To assess specificity we employed a two-window simulation protocol. During the first time window, both x and y were chosen large, corresponding to high levels of pheromone induction. We have verified that setting $y = 0$ in the first window results in almost identical results. This is not surprising, since only the activation rates for S_0 and T_0 depend on y and these rates saturate as long as x is sufficiently large. Also note that x and y have redundant roles in activating downstream kinases, e.g., Ste12. Experiments indicate that Fus3* is the dominant player in the mating program (14), although there is evidence that Kss1* is required for full mating induction (25). Since we are mainly interested in the transcription factors S_2 and T_2, additional downstream functions of Kss1* are not considered. During the second time window, x was set to zero whereas y was assigned a high value, simulating the nutritional deprivation condition. The duration of both windows was chosen long enough for steady-state responses. We do not model the desensitization of the MAPK activation (25) for two reasons. First, this desensitization occurs on timescales of several hours, much longer than the time required to reach a steady state for the transcription factor levels. Second, the activation functions (see Supporting Material) are sigmoidal functions of x and y, and will saturate as long as x and y remain above a threshold value, even if the inputs are time-varying.

To quantify the specificity of our model we use two previously introduced metrics (26,27). The first one measures simply the ratio of the S_2 and T_2 response during each window: $S_X = ln(S_2|_x/T_2|_x)$ in the first time window and $S_Y = ln(T_2|_y/S_2|_y)$ in the second. Clearly, signaling specificity is achieved when both S_X and S_Y are positive and large. The second metric is called the signaling fidelity. A large fidelity means that the activation of a pathway through its authentic upstream signal is larger than the activation resulting from cross-talk. For the S_2 signaling, it is defined as the ratio of S_2 during the first time window and S_2 during the second window: $V_X = ln(S_2|_x/S_2|_y)$. Similarly, we define the fidelity for T_2 as $V_Y = ln(T_2|_y/T_2|_x)$. Note that those metrics are mathematically related: $V_X + V_Y = S_X + S_Y$.

RESULTS

A typical example of a numerical simulation, using the default parameter set $(F_S, F_T, F_\lambda, q, w) = (2,8,4,1,1)$ together with the parameters of Table S2, is plotted in Fig. 2 *A*, which shows the output of our model (Ste12*-Ste12*, *solid line* and Tec1*-Ste12*, *dashed line*) as a function of time. Fig. 2 *B* shows the specificity measure S_X and S_Y for the time trace in Fig. 2 *A*. We have also computed the fidelity for this time trace and found that $V_X \doteq 2.5$ and $V_Y \doteq 2.0$ at steady state. Thus, our model can exhibit both signaling specificity and fidelity through the appropriate choice of parameters.

Next, we vary two of the five essential numerical parameters, while keeping the remaining three constant. Examples of these simulations are shown in Fig. 3. The first panel plots S_X and S_Y as a function of F_S and F_T. We used a grayscale with white corresponding to high values of the metric and black for the low values. Note that at the intersection between the two surfaces both metrics are ~2, indicating good specificity. In the second panel, we show similar curves for V_X and V_Y. The results are combined in the third panel in which we plot the region where $S_{X,\,Y}$ is above a threshold

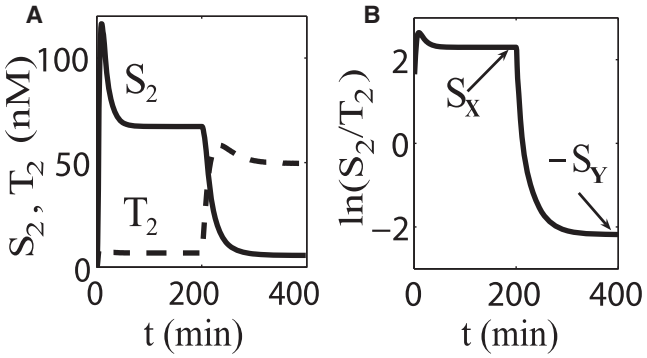

FIGURE 2 A typical numerical result using our stimulation protocol. In the first time window, the input to the mating pathway (x) is high, whereas the input to the filamentation pathway (y) is low. During the second window, the input is reversed. The durations of both windows are set to 200 min. (*A*) Time traces of our model output (activated Ste12*-Ste12* dimer, S_2, and the activated Ste12*-Tec1* dimer, T_2). (*B*) Corresponding signaling specificity S_X and S_Y computed from panel *A*.

value as open circle symbols and where $V_{X,\ Y}$ above this value as shaded dot points. Since experimental data on this threshold is not available, we have chosen here the value $ln(5)$ as an illustrative example. The overlap between the two regions, corresponding to a parameter region with both high specificity and fidelity, is represented by solid circle symbols. We have investigated the specificity and fidelity using all possible combinations of two of the five main parameters. Examples of these parameter sweeps are shown in Fig. 4, *A–D*. Again, a large region in parameter space exists where both the specificity and fidelity can be achieved. Fig. 4 *C* shows the same slice in parameter space as Fig. 4 *D*, but for $w = 0.2$. The overlap region becomes significantly larger for increasing w, illustrating the importance of an appreciable degradation rate for the dimers. We will discuss this in more detail below.

Through extensive numerical simulations, we found the following conditions necessary for signaling specificity in our model:

1. F_S, characterizing the feedback strength of S_2 on S_0, should be chosen to be smaller than F_T, which controls the feedback of T_2 on T_0. This can be seen in Fig. 3 *C*, where the overlap in parameter space is well below the line $F_S = F_T$. Fig. 3 *C* also shows that F_T needs to have a certain minimum value, which is ~5 for our chosen parameters.
2. The dimers need to have a minimal basal degradation rate. This can be seen in Fig. 4 *A*, where the overlap region (*solid*) shrinks for decreasing values of w and even disappears for $w < 0.1$. It is also shown in Fig. 4, *E* and *F*, where we plot S_2 and T_2 as well as the signaling specificity metrics during our two-window numerical experiments for $w = 0$ (completely stable dimers). During the first time window, S_2 is significantly higher than T_2. However, S_2 remains high in the second window, destroying signaling specificity as negative S_Y shown in Fig. 4 *F*.
3. For a given set of parameters, we found that the values for q that exhibit signaling specificity and fidelity are bounded by a minimum and a maximum value. This can be seen in Fig. 4, *C* and *D*, where, for fixed values of F_λ, the overlap region starts at a smaller value of q and ends at a larger q.
4. The Fus3*-mediated degradation, described by the parameter F_λ, demands a certain minimum value, found to be ~3 in simulations. This is illustrated in Fig. 4, *B–D*.

In summary, we found that signaling specificity imposed the following parameter constraints: $1 < F_S < 5 < F_T$, $F_\lambda > 3$, $w > 0.1$, and $q_{min} < q < q_{max}$, where q_{min} and q_{max} mostly depend on the choice of w and F_λ.

In addition to these parameter constraints, our simulations also exclude the bistable property, i.e., the existence of two stable steady-state solutions for the same set of parameters. Bistability was argued in a recent study to be the consequence of mutual inhibition and the resulting history-dependent output was observed in experiments probing the high osmolarity response and pheromone-induced mating in yeast (28).

To understand the absence of multiple stable steady solutions, we further reduce our four-variable model by solving Eqs. 1 and 3 for S_0 and T_0. Substituting the results into Eqs. 2 and 4 yields two nonlinear coupled ordinary differential equations:

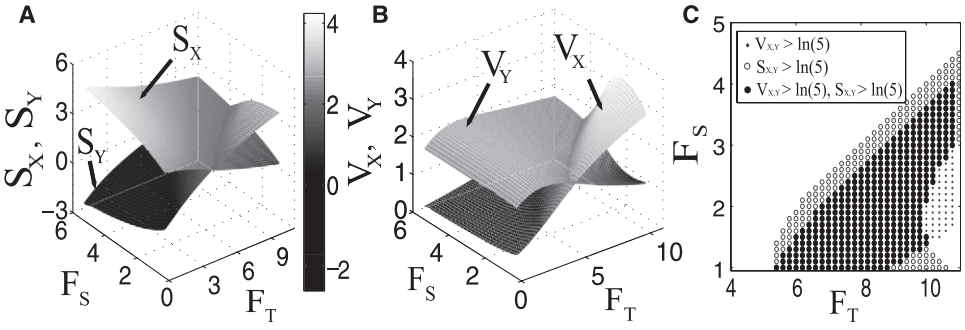

FIGURE 3 The response of our model for varying F_S and F_T. (*A*) The specificity S_X and S_Y as a function of F_S and F_T. The surface is shaded in a grayscale manner. (*B*) The fidelity V_X and V_Y as a function of F_S and F_T. (*C*) The result of a parameter sweep in F_S vs. F_T space. The parameter combination for which the specificity is larger than ln(5) is shown as open circle symbols, and where the fidelity is larger than ln(5) is shown as shaded dot symbols. The solid circle symbols correspond to parameter values for which both the specificity and the fidelity are greater than ln(5).

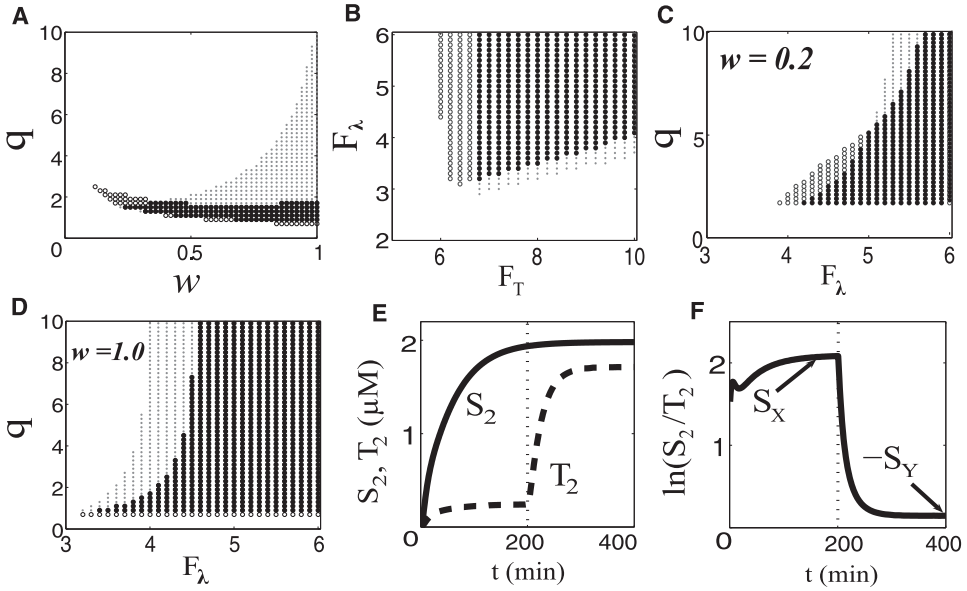

FIGURE 4 (*A–D*) The regions of high specificity and fidelity for different parameter sweeps with threshold ln(5), using the same legend as in the previous figure. (*E* and *F*) The two-window simulation results in the absence of dimer degradation ($w = 0$).

$$\frac{dS_1}{dt} = \frac{d_S S_1 + \lambda_S S_b P_S(S_2)}{1 + \lambda_S/g_S(x,y)} - d_S S_1 - \lambda_S S_1 - 2w\lambda_S S_2 - w\lambda_T(0)T_2, \tag{5}$$

$$\frac{dT_1}{dt} = \frac{d_T T_1 + \lambda_T(0) T_b P_T(T_2)}{1 + \lambda_T(x)/g_T(x,y)} - d_T T_1 - \lambda_T(x) T_1 - w\lambda_T(x) T_2, \tag{6}$$

where, as we have discussed before, S_2 and T_2 are functions of S_1 and T_1. Note that the only term that couples the two equations is $w\lambda_T(0)T_2$, which arises from the heterodimer degradation. The steady-state solution can also be found at the intersection of the nullclines of the above equations, defined as the curves in S_1 versus T_1 space for which $\frac{dS_1}{dt} = 0$ and $\frac{dT_1}{dt} = 0$. Extensive numerical exploration of parameter space reveals that these curves intersect only once. Thus, there exists a unique steady state, which rules out a history-dependent trajectory in phase space. The uniqueness of our output can also be seen in Fig. 5 *A*, where we plot S_2 and T_2 as functions of x and y. Obviously, the outputs are single-valued for this representative set of parameters. Our results are markedly different than the ones from a recent theoretical model in the Supporting Information of McClean et al. (28), which displays history-dependent bistability between mating and filamentous growth. We will comment further on the differences between the two models in Discussion.

To gain insight into the importance of nonvanishing decay of dimers $w > 0$, we then solve the steady equations for S_2 and T_2 using Eqs. 5 and 6:

$$S_2 = \frac{S_b P_S(S_2)}{2w(1 + \lambda_S/g_S)} - \left(1 + \frac{d_S}{g_S + \lambda_S}\right)\frac{S_1}{2w} - \frac{\lambda_T(0)}{2\lambda_S} T_2, \tag{7}$$

$$T_2 = \frac{\lambda_T(0)}{\lambda_T(x)} \frac{T_b P_T(T_2)}{w(1 + \lambda_T(x)/g_T)} - \left(1 + \frac{d_T}{g_T + \lambda_T(x)}\right)\frac{T_1}{w}. \tag{8}$$

Since $S_1 = \sqrt{K_S S_2}$ and $T_1 = K_T(x)T_2/S_1 = K_T(x)T_2/\sqrt{K_S S_2}$, the above two equations can be rewritten in terms of S_2 and T_2 only:

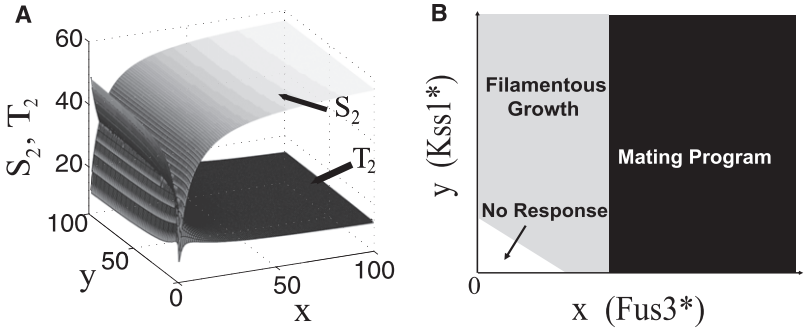

FIGURE 5 (*A*) The output of our model for a representative set of parameters. The value of S_2 and T_2 is uniquely defined for each pair of (x, y). (*B*) The schematic phase diagram of our model with white denoting no response, solid corresponding to the activation of the mating pathway, and shading labeling the activation of filamentous growth.

$$S_2 + \left(1 + \frac{d_S}{g_S + \lambda_S}\right)\frac{\sqrt{K_S S_2}}{2w} = \frac{S_2 P_S(S_2)}{2w(1 + \lambda_S/g_S)} - \frac{\lambda_T(0)}{2\lambda_S} T_2, \tag{9}$$

$$T_2 = T_b P_T(T_2)\left[\frac{\lambda_T(x)}{\lambda_T(0)}\left(1 + \frac{\lambda_T(x)}{g_T}\right) \times \left(w + \left(1 + \frac{d_T}{g_T + \lambda_T(x)}\right)\right)\frac{K_T(x)}{\sqrt{K_S S_2}}\right]^{-1}. \tag{10}$$

In Eq. 9, the last term represents the draining effect of Tec1 on Ste12 reservoir due to the turnover of Tec1*-Ste12*. This effect ensures that when y is large and x is very low, the level of S_2 remains low and the mating pathway is suppressed. Note that this term becomes negligible when $w \to 0$, leading to high levels of S_2 in the presence of large y and small x, and thus to the destruction of specificity for the filamentation pathway.

This draining effect is also controlled by the parameter q, which appears implicitly in these equations through $K_T(x)$ since $K_T(x) \sim 1/q$. Therefore, T_2 in equilibrium is proportional to q and choosing large values of q will increase the draining effect. However, even though large q promotes specificity in the filamentation pathway, it may ruin the specificity for the mating pathway. This can be seen by realizing that for large x and small w, the output T_2 is approximately proportional to q/F_λ. Thus, there is a trade-off between the heterodimerization rate and the degradation rate of T_2 (Fig. 4 *A*), and choosing large values of q may potentially produce high T_2 output even at high concentrations of Fus3*.

Our results can be schematically summarized in the phase diagram in Fig. 5 *B*. At low concentrations of Fus3* and Kss1*, the model response is low in both S_2 and T_2 (see also Fig. 5 *A*). In the open region of Fig. 5 *B*, these levels are probably too small to activate either pathway. Upon increasing the level of Kss1* while maintaining a low level of Fus3*, it will activate the filamentous growth pathway (*shaded region*). Once the Fus3* level has crossed a certain threshold, the mating program is initiated (*solid region*) while the filamentation program is suppressed. This threshold in x is also clear in Fig. 5 *A* and largely independent of y. Therefore, Fus3 seems to be the determining factor for pathway specificity, consistent with experimental results and previous arguments (14).

DISCUSSION

Mechanisms of our model

The goal of any specificity model for the mating and filamentation pathways should be to give high S_2 (Ste12*-Ste12*) output levels and low T_2 (Tec1*-Ste12*) levels in the presence of high x (Fus3*)/low y (Kss1*) and the reverse for high y/low x input. How is this accomplished in our model? High values of Fus3* lead to increased activation rates of Ste12 but also of Tec1. The latter, however, is suppressed because of the Fus3*-mediated degradation (controlled by F_λ). The result is a high level of S_2 and a low level of T_2. Note, however, that the heterodimerization process, controlled by the parameter q, cannot be too large (Fig. 4 *C*). The relatively high rate of heterodimerization, i.e., large q, can potentially overcome the enhanced degradation rates and may bring high T_2 output even in pheromone signaling.

High concentrations of Kss1* in response to nutritional starvation also trigger the activation of Ste12 and Tec1, which further form dimers. The heterodimer T_2 is degraded at a rate controlled by the parameter w, balanced by de novo synthesis of Tec1 and new formation of heterodimer. As long as w is larger than a certain threshold, this degradation/synthesis cycle functions as a continuing drain on the Ste12 reservoir, finally reducing the S_2 output. Similarly, q also has a minimum bound (Fig. 4, *C* and *D*), below which the heterodimerization could be too slow to effectively absorb and drain the Ste12 reservoir. Furthermore, the genetic positive feedback of Tec1, controlled by the parameter F_T, enlarges the Tec1 reservoir and amplifies its draining capacity on Ste12 resource. Consequently, choosing F_T too small will weaken this draining effect and cause erroneous cross-activation. In addition, the positive feedback loop containing S_2, tuned by F_S, boosts the levels of S_2. For large values of F_S, this feedback can be sufficient to overcome the draining effect and impair specificity. Hence, there is a constraint on the values of F_S, as seen in Fig. 3 *C*.

From the above, we conclude that the asymmetric hierarchical inhibitions in our model are crucial for yeast signaling specificity. Asymmetric, since the three crucial processes described earlier break the symmetry between the mating and filamentation pathway; and hierarchical, since the inhibitory effect of Fus3* on Tec1 works at a higher level of the pathway and depends only weakly upon the genetic feedback regulation. This is in contrast to the draining effect by the dimer degradation, which operates at a pathway level that is further downstream. As a consequence, the decision of yeast cell fate is made hierarchically. At the top of the decision tree, the concentration of Fus3* is evaluated: regardless of the level of Kss1*, high Fus3* will drastically reduce the Tec1 pool and direct the cell to the mating program. For low concentrations of Fus3*, the Fus3-dependent inhibitory effect is weak, and the level of Kss1* is evaluated further down the decision tree: at high Kss1*, the draining effect by Tec1*-Ste12* becomes dominant and the filamentous growth pathway is activated. Our proposed hierarchical inhibition mechanism is different from the mutual inhibition mechanism observed where the inhibition usually occurs at the same level or appears symmetric in the signaling pathways. An example can be found in the yeast osmolar and pheromone responses where the MAPKs Fus3 and Hog1 inhibit each other after activation. This mutual inhibition mechanism may easily lead to bistable behavior as observed recently (28). In contrast, the hierarchical inhibition mechanism may not favor bistable property in nature, as characterized in Fig. 5 *B*.

Our deterministic model is based, where possible, on known signaling components and their interactions. The kinetic rates are, for the most part, taken from experimental data. However, we should note that most experiments to date have used biochemical methods that obtain population-averaged results. It is clear that there can be significant cell-to-cell variability, arising from either the fluctuations of protein levels or the stochasticity of protein interactions. As an example of this, considerable variations in the levels of MAPK Fus3 and Kss1 have recently been documented (29). Thus, one may be concerned that the parameter values used here might not accurately reflect single cell behavior; this might be the case if, for instance, only a small fraction of the cells respond to external stimuli (30). Obviously, the inclusion of these uncertainties is beyond the scope of our current model, but could be included in future extensions.

Comparison with previous models

Two recent models for the mating and filamentation pathway rely on a mutual inhibitory interaction that takes into account a drop of Tec1 level in the presence of Fus3* and the draining effect by the heterodimerization process (without dimer degradation) on the Ste12 resource (28,31). There are, however, several significant differences between these models and ours.

First, the parameter values in our model are, where possible, based on experimental data, whereas the parameters in the model in McClean et al. (28) appear to be chosen more freely. Thus, one should be able to compare the results of our model directly to experimental results.

Second, the Tec1 genetic feedback was taken to be linearly dependent on the concentration of Tec1*-Ste12* in McClean et al. (28), and could reach arbitrary values in principle. Thus, the draining effect by heterodimerization alone can be sustained and unlimited. In the study by Chou et al. (31), this draining effect was achieved by assuming that the total Ste12 concentration is constant. Thus, the formation of the heterodimers automatically depletes the Ste12 resource.

In our model, we have a sigmoidal feedback for both the Tec1 and Ste12 gene expression, which leads to qualitatively different behavior. Remarkably, the draining effect through heterodimerization by itself becomes transient and limited when the genetic feedback of Tec1 expression is saturated. Hence, an additional mechanism needs to be incorporated to establish and maintain a continuing drain on the Ste12 resource. We argue here that the heterodimer degradation might provide such a mechanism to couple with the heterodimerization process. As long as this degradation is large enough, there will be an outflux from Ste12* to Tec1*-Ste12*, preventing the buildup of Ste12*-Ste12* and ensuring the signaling specificity at high concentrations of Kss1*.

We have verified through simulations that replacing the sigmoidal feedback in our model with a linear version gives rise to bistable behavior; even when $w = 0$, i.e., dimers are completely stable. Furthermore, we have performed simulations of the model in McClean et al. (28) using our two-window protocol. We found that the existence of bistability depends critically on the strength of the feedback, and that reducing this strength more than threefold from the parameter value in McClean et al. (28) leads to monostable behavior. Thus, the history-dependent bistability found in McClean et al. (28) is likely a parameter-dependent phenomenon and may not be a natural result of the cross-pathway mutual inhibition. This difference in qualitative outcomes is a key feature that distinguishes our model from previous ones, and should be accessible through experiments, as the outcome of the bistable system will be history dependent, whereas our model predicts a unique outcome, independent of the input history. Although a future experiment in favor of our prediction does not prove our model, such a result will favor the conceptual framework proposed here over competing concepts based on symmetric cross-pathway inhibition.

In summary, our model efficiently simplifies the highly complex signaling network and clearly provides a quantitative understanding of this complicated cellular decision system. Our approach highlights the key interactions and predicts the parameter ranges consistent with known experiments. Finally, by introducing the asymmetric hierarchical inhibition, it offers an alternative to the traditional symmetric mutual inhibition mechanism.

Comparison with experiments

Our model is able to capture a number of experimental observations.

First, eliminating the Fus3*-mediated Tec1 degradation, accomplished by setting $F_\lambda = 1$, destroys the specificity in our model. This can be seen, for example, in Fig. 4 *B* where the region with both high specificity and fidelity requires a minimum value of F_λ. For reasonably large values of F_T, the abolishment of Fus3*-mediated Tec1* degradation results in the activation of the filamentous growth pathway. This agrees with experiments in which $Tec1^{T273V}$ blocks Tec1 ubiquitination and degradation and allows the induction of filamentation genes in response to pheromone (14).

Second, the signaling specificity in our model breaks down for $F_S > F_T$ (Fig. 3 *C*). In other words, a requirement for specificity is that the Tec1 genetic feedback is stronger than the Ste12 genetic feedback. This agrees with recent measurements of yeast gene expression, which show that Ste12 is weakly upregulated by its dimers, whereas the positive feedback on Tec1 is stronger (23).

Third, the level of Fus3* is the determining factor in the cell's fate. This is consistent with experimental documents suggesting that Fus3 is capable of all functions that Kss1 is known for (14). Note that Fus3 has additional mating specific functions, such as pheromone-induced G1 phase arrest, polarity formation for shmooing, and maintaining pathway specificity via degrading Tec1. The additional functions of Fus3 may

explain why Fus3 activation has to be under tight control in vivo and is strictly dependent on the Ste5 scaffold (32).

Experimental predictions

Several predictions can be made on the basis of our model, some of which may be experimentally accessible. First of all, our model predicts that the stability of heterodimer Tec1*-Ste12* critically affects the level of filamentation gene expression. In our model, this is controlled by the parameter w. Decreasing w significantly elevates the levels of both S_2 and T_2, whereas choosing w close to zero endangers signaling specificity (Fig. 4, *E* and *F*). Recent experiments have shown the ability to obtain tunable degradation of a tagged protein through a synthetic gene network in *Saccharomyces cerevisiae* (33). Our predictions about dimer stability may be testable using similar experimental techniques in the future.

In addition, overactivation of Kss1 in the presence of pheromone stimulation will not result in filamentous differentiation. This can be most easily seen in the phase diagram, which shows that, even for large values of Kss1*, the Fus3* determines the outcome. In addition, overexpression of *STE12* by its transcription homodimer, corresponding to choosing $F_S >> 1$ in the model, may destroy the filamentation signaling specificity. This is shown in Fig. 3 *C*, where keeping F_T fixed and increasing F_S is demonstrated to lose specificity. Conversely, and also shown in Fig. 3 *C*, overexpression of *TEC1* by its transcription heterodimer, i.e., $F_T >> F_S$, may kill the mating signaling specificity.

Finally, we predict a single steady-state solution, which is reached in a history-independent fashion. Hence, the final outcome should be the same regardless of the sequence of external cues given to the cell. Perhaps experiments similar to the ones in McClean et al. (28) are possible to determine the trajectory in phase space, and should contribute to our understanding of the underlying mechanisms for eukaryotic signaling specificity.

SUPPORTING MATERIAL

Two tables and two figures are available at http://www.biophysj.org/biophysj/supplemental/S0006-3495(09)00674-2.

We thank Dr. Lee Bardwell for a critical reading of the manuscript and valuable comments.

This research has been supported by the National Science Foundation-sponsored Center for Theoretical Biological Physics (grant Nos. PHY-0216576 and PHY-0225630).

REFERENCES

1. Schwartz, M. A., and H. D. Madhani. 2004. Principles of MAP kinase signaling specificity in *Saccharomyces cerevisiae*. *Annu. Rev. Genet.* 38:725–748.
2. Liu, H., C. A. Styles, and G. R. Fink. 1993. Elements of the yeast pheromone response pathway required for filamentous growth of diploids. *Science.* 262:1741–1744.
3. Roberts, R. L., and G. R. Fink. 1994. Elements of a single MAP kinase cascade in *Saccharomyces cerevisiae* mediate two developmental programs in the same cell type: mating and invasive growth. *Genes Dev.* 8:2974–2985.
4. Schaeffer, H. J., and M. J. Weber. 1999. Mitogen-activated protein kinases: specific messages from ubiquitous messengers. *Mol. Cell. Biol.* 19:2435–2444.
5. Elion, E. A. 2000. Pheromone response, mating and cell biology. *Curr. Opin. Microbiol.* 3:573–581.
6. Cook, J. G., L. Bardwell, S. J. Kron, and J. Thorner. 1996. Two novel targets of the MAP kinase Kss1 are negative regulators of invasive growth in the yeast *Saccharomyces cerevisiae*. *Genes Dev.* 10:2831–2848.
7. Yuan, Y. L., and S. Fields. 1991. Properties of the DNA-binding domain of the *Saccharomyces cerevisiae* STE12 protein. *Mol. Cell. Biol.* 11:5910–5918.
8. Olson, K. A., C. Nelson, G. Tai, W. Hung, C. Yong, et al. 2000. Two regulators of Ste12p inhibit pheromone-responsive transcription by separate mechanisms. *Mol. Cell. Biol.* 20:4199–4209.
9. Madhani, H. D., and G. R. Fink. 1998. The control of filamentous differentiation and virulence in fungi. *Trends Cell Biol.* 8:348–353.
10. Pan, X., T. Harashima, and J. Heitman. 2000. Signal transduction cascades regulating pseudohyphal differentiation of *Saccharomyces cerevisiae*. *Curr. Opin. Microbiol.* 3:567–572.
11. Gancedo, J. M. 2001. Control of pseudohyphae formation in *Saccharomyces cerevisiae*. *FEMS Microbiol. Rev.* 25:107–123.
12. Madhani, H. D., and G. R. Fink. 1997. Combinatorial control required for the specificity of yeast MAPK signaling. *Science.* 275:1314–1317.
13. Brückner, S., T. Köhler, G. H. Braus, B. Heise, M. Bolte, et al. 2004. Differential regulation of Tec1 by Fus3 and Kss1 confers signaling specificity in yeast development. *Curr. Genet.* 46:331–342.
14. Chou, S., L. Huang, and H. Liu. 2004. Fus3-regulated Tec1 degradation through SCFCdc4 determines MAPK signaling specificity during mating in yeast. *Cell.* 119:981–990.
15. Bao, M. Z., M. A. Schwartz, G. T. Cantin, J. R. Yates, III, and H. D. Madhani. 2004. Pheromone-dependent destruction of the Tec1 transcription factor is required for MAP kinase signaling specificity in yeast. *Cell.* 119:991–1000.
16. Zeitlinger, J., I. Simon, C. T. Harbison, N. M. Hannett, T. L. Volkert, et al. 2003. Program-specific distribution of a transcription factor dependent on partner transcription factor and MAPK signaling. *Cell.* 113:395–404.
17. Harris, K., R. E. Lamson, B. Nelson, T. R. Hughes, M. J. Marton, et al. 2001. Role of scaffolds in MAP kinase pathway specificity revealed by custom design of pathway-dedicated signaling proteins. *Curr. Biol.* 11:1815–1824.
18. Park, S. H., A. Zarrinpar, and W. A. Lim. 2003. Rewiring MAP kinase pathways using alternative scaffold assembly mechanisms. *Science.* 299:1061–1064.
19. Flatauer, L. J., S. F. Zadeh, and L. Bardwell. 2005. Mitogen-activated protein kinases with distinct requirements for Ste5 scaffolding influence signaling specificity in *Saccharomyces cerevisiae*. *Mol. Cell. Biol.* 25:1793–1803.
20. Chou, S., S. Lane, and H. Liu. 2006. Regulation of mating and filamentation genes by two distinct Ste12 complexes in *Saccharomyces cerevisiae*. *Mol. Cell. Biol.* 26:4794–4805.
21. Wang, Y., and H. G. Dohlman. 2006. Pheromone-regulated sumoylation of transcription factors that mediate the invasive to mating developmental switch in yeast. *J. Biol. Chem.* 281:1964–1969.
22. Esch, R. K., Y. Wang, and B. Errede. 2006. Pheromone-induced degradation of Ste12 contributes to signal attenuation and the specificity of developmental fate. *Eukaryot. Cell.* 5:2147–2160.
23. Ren, B., F. Robert, J. J. Wyrick, O. Aparicio, E. G. Jennings, et al. 2000. Genome-wide location and function of DNA binding proteins. *Science.* 290:2306–2309.
24. Gasch, A. P., P. T. Spellman, C. M. Kao, O. Carmel-Harel, M. B. Eisen, et al. 2000. Genomic expression programs in the response of yeast cells to environmental changes. *Mol. Biol. Cell.* 11:4241–4257.

25. Sabbagh, W., L.J. Flatauer, A.J. Bardwell, and L. Bardwell. Specificity of MAPK signaling in yeast differentiation involves transient vs. sustained MAPK activation. Mol. Cell. 8:683–691.

26. Komarova, N. L., X. Zou, Q. Nie, and L. Bardwell. 2005. A theoretical framework for specificity in cell signaling. *Mol. Syst. Biol.* 1, 2005.0023.

27. Bardwell, L., X. Zou, Q. Nie, and N. L. Komarova. 2007. Mathematical models of specificity in cell signaling. *Biophys. J.* 92:3425–3441.

28. McClean, M. N., A. Mody, J. R. Broach, and S. Ramanathan. 2007. Cross-talk and decision making in MAP kinase pathways. *Nat. Genet.* 39 (Suppl.):409–414.

29. Colman-Lerner, A., A. Gordon, E. Serra, T. Chin, O. Resnekov, et al. 2005. Regulated cell-to-cell variation in a cell-fate decision system. *Nature*. 437:699–706.

30. Halme, A., S. Bumgarner, C. Styles, and G. R. Fink. 2004. Genetic and epigenetic regulation of the FLO gene family generates cell-surface variation in yeast. *Cell.* 116:405–415.

31. Chou, S., S. Zhao, Y. Song, H. Liu, and Q. Nie. 2008. Fus3-triggered Tec1 degradation modulates mating transcriptional output during the pheromone response. *Mol. Syst. Biol.* 4:212.

32. Andersson, J., D. M. Simpson, M. Qi, Y. Wang, and E. A. Elion. 2004. Differential input by Ste5 scaffold and Msg5 phosphatase route a MAPK cascade to multiple outcomes. *EMBO J.* 23:2564–2576.

33. Grilly, C., J. Stricker, W. L. Pang, M. R. Bennett, and J. Hasty. 2007. A synthetic gene network for tuning protein degradation in *Saccharomyces cerevisiae*. *Mol. Syst. Biol.* 3:127.